AD_____

Award Number: W81XWH-07-1-0065

TITLE: Effects of Radiation on Proteasome Function in Prostate Cancer Cells

PRINCIPAL INVESTIGATOR: Frank Pajonk, M.D., Ph.D.

CONTRACTING ORGANIZATION: University of California
Los Angeles, CA 90024

REPORT DATE: February 2009

TYPE OF REPORT: Annual Summary

PREPARED FOR: U.S. Army Medical Research and Materiel Command
Fort Detrick, Maryland 21702-5012

REPORT DOCUMENTATION PAGE

Form Approved
OMB No. 0704-0188

1. REPORT DATE	**2. REPORT TYPE**	**3. DATES COVERED**
1 Feb 2009	Annual Summary	15 Jan 2008 – 14Jan 2009

4. TITLE AND SUBTITLE

Effects of Radiation on Proteasome Function in Prostate Cancer Cells

5a. CONTRACT NUMBER

5b. GRANT NUMBER
W81XWH-07-1-0065

5c. PROGRAM ELEMENT NUMBER

6. AUTHOR(S)

Frank Pajonk, M.D., Ph.D.

E-Mail: fpajonk@mednet.ucla.edu

5d. PROJECT NUMBER

5e. TASK NUMBER

5f. WORK UNIT NUMBER

7. PERFORMING ORGANIZATION NAME(S) AND ADDRESS(ES)

University of California
Los Angeles, CA 90024

8. PERFORMING ORGANIZATION REPORT NUMBER

9. SPONSORING / MONITORING AGENCY NAME(S) AND ADDRESS(ES)
U.S. Army Medical Research and Materiel Command
Fort Detrick, Maryland 21702-5012

10. SPONSOR/MONITOR'S ACRONYM(S)

11. SPONSOR/MONITOR'S REPORT NUMBER(S)

12. DISTRIBUTION / AVAILABILITY STATEMENT
Approved for Public Release; Distribution Unlimited

13. SUPPLEMENTARY NOTES

14. ABSTRACT

Not provided

15. SUBJECT TERMS
Prostate Cancer

16. SECURITY CLASSIFICATION OF:			**17. LIMITATION OF ABSTRACT**	**18. NUMBER OF PAGES**	**19a. NAME OF RESPONSIBLE PERSON**
a. REPORT	**b. ABSTRACT**	**c. THIS PAGE**			USAMRMC
U	U	U	UU	25	**19b. TELEPHONE NUMBER** *(include area code)*

Table of Contents

Introduction

The proposed research is based on our observation that the 26S proteasome is a direct target of radiation.
We initially planned experiments to investigate the association and release of PIPs from the 26S proteasome as well as studies more focused on the structural changes of the proteasome in response to radiation. We also wanted to investigate how the 26S is regulated by radiation at the transcriptional and posttranslational level and we are addressing these aims using powerful proteomic tools.

Body

In order to answer the question (Aim 1.a) if irradiation cause ATP-dependent release/retention of PIPs we use an approach, which allows us to get clear snapshot of the entire system. As already described in the previous progress report we were able to establish immunoprecipitation of the purification of 26S proteasomes, thereby overcoming the shortcomings of glycerol gradient purification. We reached this goal through collaboration with Dr. Lan Huang from UC Irvine, who provided us with an expression vector for a tagged Rpn11 protein (Rpn11-6xHIS-TEV-Biotin-6xHis). Briefly, cells were lyzsed and irradiated (10Gy) on ice, next. Using magnetic streptavidin-conjugated beads (Invitrogen), that bind to biotin tagged proteins, we pulled down the 26S proteasome (Fig. 1). Using *TEV*, a specific protease that recognizes the sequence Glu-Asn-Leu-Tyr-Phe-Gln-Gly and cleaves between the Gln and Gly residues, we removed the beads obtaining "clean" 26S preparations. The purity of the proteasome 26S complex by was verified by electrophoresis. Both, irradiated and not treated samples were run through an acrylammide gel (SDS-PAGE) and the 26S subunits were visualized by Coomassie Briliant Blue staining.
In order to demonstrate the robustness of our purification method we also performed immunoprecipitations using another prostate cancer cell line (DU145).
Figure 1 shows an example of SDS-PAGE stained with Coomassie Brilliant Blue performed on the 26S preparations on PC3 cells. In order to characterize the proteins and the subunits, all bands from the lanes of treated and non-treated samples were excided from the gel and digested with trypsin. Briefly, each band was dehydratated and rehydrated using acetonitrile and ammonium bicarbonate, respectively, treated with dithiothreitol (DTT) and iodoacetamide to reduce disolfure bounds, digested overnight with trypsin and finally eluted from the gel using a solution of formic acid/acetonitrile. Tryptic digests were dried down (Speedvac) in order to concentrate the peptides and either stored at -80 or analyzed right away by mass spectrometry using a Fourier-transform ion cyclotron resonance mass spectrometry (FT-MS) (Pasarow Mass Spectrometry Laboratory, UCLA). The high sensitivity of this instrument allowed us to characterize the proteins contained in the bands, identifying the subunits composition, and detecting any change in their composition (presence/absence) due to the radiation exposure (Tabel 1). Computational mass spectrometry (UCSD) and OMSSA browsers were used for data analysis.

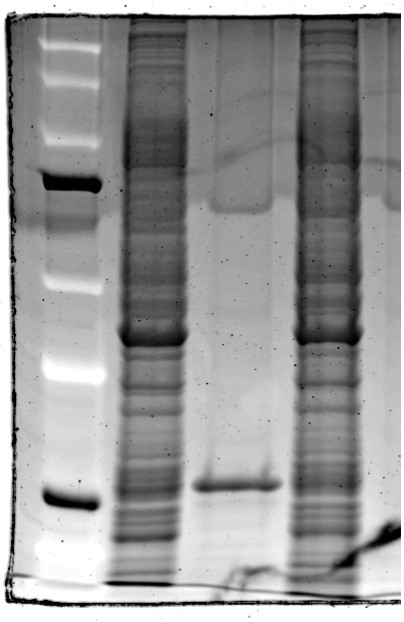

Figure 1. 10% SDS-PAGE of immunoprecipitated 26S proteasome from PC3 cell line. From the left: non-irradiated sample, TEV protease used to get off the beads, on the right irradiated samples (one dose of 10 Gy). Bands excided from both lanes on the gel were analyzed by mass spectrometry and characterized.

Table 1. List of proteins differently expressed in non-irradiated (left column) and irradiated samples (right column) divided in different groups based on their function. Data were analyzed with an FT/MS instrument.

	PC3 NON-IRRADIATED	PC3 IRRADIATED
DNA repair	ATP-binding cassette, sub-family A, member 6	APEX nuclease
	RAB7, member RAS oncogene family	minichromosome maintenance complex component 6
	RuvB-like 1	structural maintenance of chromosomes 2-like 1
Metabolism	acyl-CoA thioesterase 7 isoform hBACHd	5'-methylthioadenosine phosphorylase
	acyl-Coenzyme A binding domain containing 3	UDP-glucose ceramide glucosyltransferase-like 1 isoform 1, 2
	ATPase, H+ transporting, lysosomal 70kD, V1 subunit A, isoform 1	UDP-glucose dehydrogenase
	fumarate hydratase precursor	acyl-Coenzyme A oxidase 1, palmitoyl isoform a, b
	guanine monophosphate synthetase	adenine phosphoribosyltransferase isoform a
	biliverdin reductase B (flavin reductase (NADPH)	alpha-N-acetylglucosaminidase precursor
	leukotriene A4 hydrolase	arylacetamide deacetylase-like 1
	acyl-CoA thioesterase 7 isoform hBACHd	carboxylesterase 2 isoform 1, 1
	acyl-Coenzyme A binding domain containing 3	catalase
	aldehyde dehydrogenase 3 family, member A1	glucosamine-phosphate N-acetyltransferase 1
	fumarate hydratase precursor	glutamine-fructose-6-phosphate transaminase 2
	GCN1 general control of amino-acid synthesis 1-like 1	glutathione S-transferase M3
	hexokinase 1 isoform HKI	glycogen phosphorylase, liver

	isochorismatase domain containing 1	glycyl-tRNA synthetase
	tryptophanyl-tRNA synthetase isoform a	glyoxalase domain containing 4
		hexokinase 2
		membrane alanine aminopeptidase precursor
		methionine adenosyltransferase II, alpha
		nardilysin (N-arginine dibasic convertase) isoform a, b
		nucleoside phosphorylase
		thioredoxin domain containing 5 isoform 2
Translation/ Transcription	ribosomal protein L19, L24l L26, L27a, S13, S3a	similar to 40S ribosomal protein SA (p40) (34/67 kDa laminin receptor)
Transcription	eukaryotic translation initiation factor 5A-like 1	ribosomal protein L10
	eukaryotic translation termination factor 1	archain
	RNA binding motif protein 8A	eukaryotic translation elongation factor 1 beta 2
	DEAD (Asp-Glu-Ala-Asp) box polypeptide 5, 6	mRNA decapping enzyme
		mitochondrial ribosomal protein L11 isoform a
		ribosomal protein L10, 11, 17, 3, S11, S15, S7
Cell signaling	adhesion regulating molecule 1 precursor [Homo sapiens]	BCL2-associated athanogene 3
	adhesion regulating molecule 1 precursor	CD44 antigen
	heat shock 27kDa protein 1	DnaJ (Hsp40) homolog, subfamily A, B member 1
	exportin 5	FERM and PDZ domain containing 2 isoform 1, 3
	calnexin precursor	RAB11B, member RAS oncogene family
	calpain, small subunit 1	RW1 protein
	destrin isoform a, b	Ras-related protein Rab-11A
	dystonin isoform 1	adaptor-related protein complex 3, delta 1
	p21-activated kinase 2	annexin IV
	adaptor-related protein complex 3, sigma 1 subunit	diaphanous 1 isoform 1, 2
	heme binding protein 1	epsin 4
	kinectin 1 isoform a, b, c	fermitin family homolog 2
	kinesin family member 14	gelsolin-like capping protein
	heat shock 27kDa protein 1	heat shock 70kDa protein 9 precursor
	protein phosphatase 1	heterogeneous nuclear ribonucleoprotein A3, D, F, K
	N-myc downstream regulated gene 1	hornerin
		importin 4
		laminin, gamma 2 isoform a, b precursor
		mitogen-activated protein kinase 1
		opioid growth factor receptor-like 1
		p47 protein isoform a
		ras homolog gene family, member A, C
		regulator of G-protein signalling 19 interacting protein 1 isoform 1
		unactive progesterone receptor, 23 kD
Others	anterior gradient 2 homolog	ARP3 actin-related protein 3 homolog
	GRAM domain containing 1C	coatomer protein complex, subunit zeta 1
	NME1-NME2 protein	cofilin 2

	mel transforming oncogene	cytoplasmic FMR1 interacting protein 1 isoform a
	karyopherin alpha 2	cytoskeleton associated protein 1
	kinectin 1 isoform a, b, c	annexin IV
	stathmin 1	microtubule-associated protein, RP/EB family, member 1
	testin isoform 1, 2	radixin
	vesicle amine transport protein 1	sine oculis homeobox homolog 3
	ferritin, heavy polypeptide 1	tubulin, alpha 1a
	ribophorin I precursor	vacuolar protein sorting 35
	kinesin family member 14	replication protein A1, 70kDa
		nuclear distribution gene C homolog
		melanoma antigen family D, 2
		tumor protein D52-like 2 isoform a
Proteasome	proteasomal ATPase-associated factor 1	proteasome (prosome, macropain) activator subunit 4
	proteasome 26S non-ATPase subunit 13 isoform 2	proteasome 26S non-ATPase subunit 10 isoform 1
	ubiquitin carboxyl-terminal esterase L3	protocadherin 21 precursor
	ubiquitin protein ligase E3A isoform 1, 2	ubiquitin protein ligase E3A isoform 3
	ubiquitin specific protease 14 isoform b	
	ubiquitin-conjugating enzyme E2O	

Previously, we identified a component of the mammalian homolog of the GroEL chaperonin protein in the radiation-treated sample suggesting its association with the 26S proteasome. We confirmed the interaction between this protein and the 26S proteasome, however, we found it also in the non-irradiated samples, indicating its general association with this protease.

Our results obtained using the PC3 cell line so far demonstrated the efficiency of the method established in isolating the 26S proteasome complex from the crude lysates and the suitability of this approach. However, based on the huge quantity of identified proteins, typically coming out of a Fourier mass spectrometer, and in order to provide sizeable data of statistical significance these experiments need to be repeated several more times to exclude random effects.

The composition of the human 26S proteasome has been only recently taken into consideration and the literature still contains only a few publications on this topic. Wang and colleagues in 2007 reported a mass-spectrometic analysis of the mammalian 26S proteasome from non-malignant HEK 293 cells, reporting three new subunits and giving a map of novel phosphorylation sites for the 26S proteasome. Our study will provide a detailed description of all the proteins that in some way interact with the 26S in a prostate cancer cell line and how they differ after radiation exposure.

To study 26S proteasome subunit composition and the PIPs' impact on the activity of this protease after irradiation, we previously planned to perform 2DE gels on 26S proteasome preparations. However, based on the encouraging results already obtained with SDS-PAGE followed by mass spectrometry analysis and in order to elucidate the posttranslational modification on the 26S and the proteins associated to it, we decided to perform a 26S proteasome analysis via liquid chromatography followed by mass spectrometry (LC/MS/MS). This approach represents an elegant way to study of the intact mass of the proteins and their posttranslational modifications. The 26S preparations will be concentrated, desalted, precipitated in chloroform and ethanol and injected into an HPLC instrument coupled with a mass spectrometer (LC/MS). We have set up the conditions for the chromatography using a non-polar stationary phase and an aqueous, moderately polar, mobile phase added to trifluoroacetic acid to analyze the column eluent. We took samples subjected to radiation (10Gy) and samples non irradiated, pulled down the proteasome as described above and separately run the two samples on

the LC system. Figure 2 shows some preliminary data obtained on a PC3 sample consisting in a typical chromatogram of the 26S proteasome. The subunits are eluted with a retention time from 30 to 60 minutes.

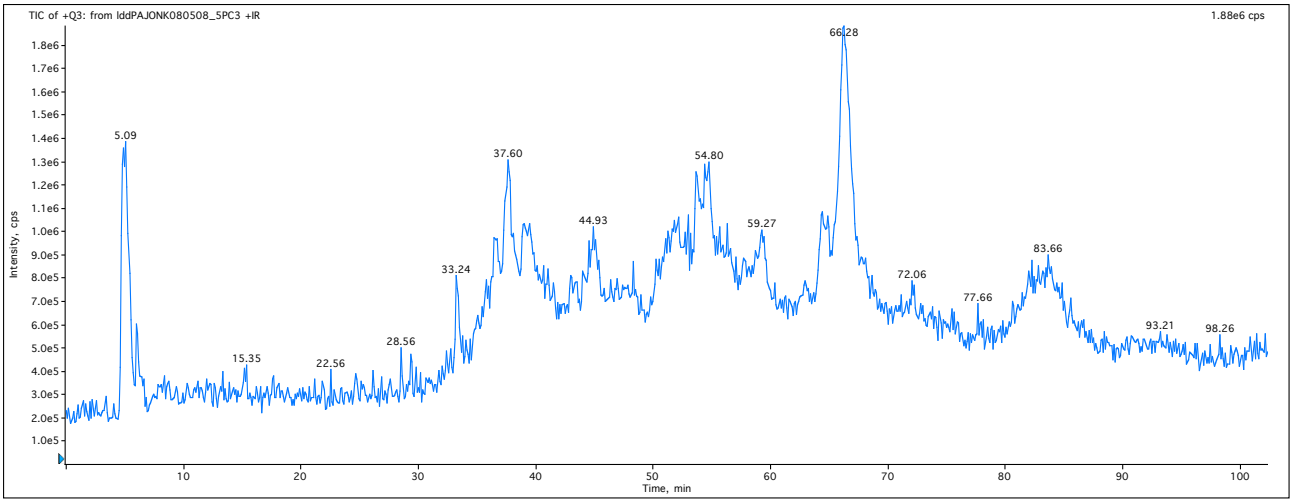

Figure 2 Chromatogram of a reverse phase chromatography on 26S preteasome preparations of PC3 cells exposed to radiation treatment (10Gy). Data were analyzed with Biomultiview Software.

Deconvolution (convertion of the mass charge ratio (m/z) in exact masses) of the raw mass spec data was performed using the Biomultiview 1.3.1 software, which gave us the precise molecular masses of each peaks. The comparison between non-irradiated and irradiated samples would have allowed us to observe a shift in the masses, which would have represented the presence of a posttranslational modification. However, due to the similarity of the two samples (irradiated and non irradiated) and most of all because of the complexity of the 26S proteasome whose subunits are often very similar to each other in terms of molecular weight and polarity, it turned out very hard to detect differences.
In order to be able to "read the chromatogram" and assign a protein name to each peak, a fraction collection system, which directs a sample eluent from the LC column through a flow splitter to the mass spectrometer was set up. All fractions, for a total of 100 fractions/sample, were collected every minute and digested with trypsin. Each fraction was analyzed by a FT/MS instrument. Data obtained from the fractions digestion and FT/MS analysis were analyzed by FT/MS. The LC system was set right before the peptides enter into the mass spectrometer and the mass spectrometer's parameters were set up with a protocol appropriate for the phosphorylation study. Unfortunately, this protocol has a high sensitivity for the phospho-peptides but it looses sensitivity for any other protein passing through it. Data were analyzed by Computational Mass Spectrometry (UCSD) and OMSSA. Our results showed a limited number of proteins and, unfortunately, just a few of them were phosphorylated. The lack of phosphorylation and the few proteins identified were due to the fact that we employed a too strict protocol and that we didn't enrich our samples in phospho-peptides.
On the basis of these results, we next decided to develop a protocol for the phospho-peptide enrichment. In a different experiment we pulled down the 26S proteasome and we performed SDS-PAGE on irradiated (10Gy) and non treated 26S proteasomes. After having checked the profile of the 26S proteasome gel we stained it with Coomassie Brilliant Blue, cut all lanes into slices and digested them with trypsin. In order to get as many phosphopeptides as possible, this time we passed each digested sample through a specific column made of titanium oxide. We have actually set up the method in collaboration with the core facility (Pasarow Mass Spectrometry at UCLA) and we are currently working on the protein identifications. This study partially addressed the leading question of our proposal: whether posttranslational modifications of the 26S proteasome and PIPs are induced by irradiation.

Aim 1.a proposed to investigate the role of ATP on 26S proteasome preparations, in particular after irradiation.
In order to address this aim, we performed immunoprecipitations that allowed us to pull down the proteasome followed by SDS-PAGEs separation. Figure 3 shows preliminary data. Bands digestion and analysis by mass

spectrometry helped us to elucidate how the 26S activity is modulated in presence/absence of ATP before and after irradiation.

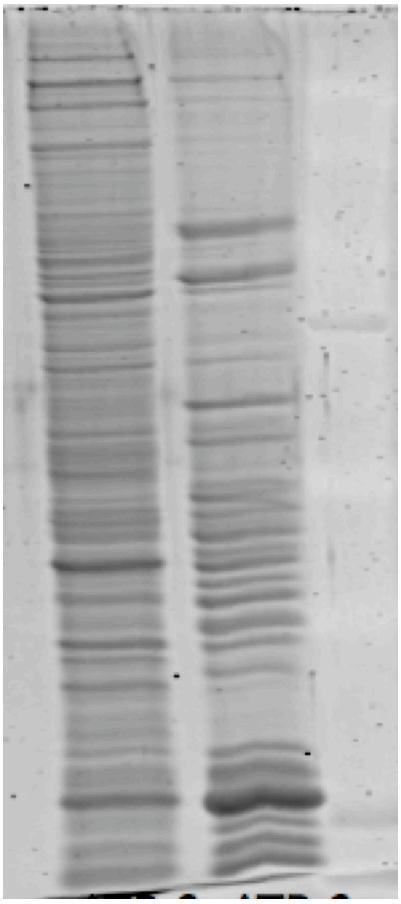

Figure 3. 10% SDS-PAGE of immunoprecipitated 26S proteasome from PC3 cells extracted with ATPγS instead of ATP. From the left: not irradiated sample; irradiated sample (single dose of 10 Gy). Bands excided from both lanes on the gel (A and B) were analyzed by mass spectrometry and characterized.

This approach allowed us to look at the differences in the PIPs profile. As shown in figure 3, even in the SDS-PAGE irradiated and non-irradiated sample differed substantially. In order to characterize all the proteins present in these bands we digested them with trypsin, cutting each band from the two lanes (treated versus untreated) and we run them on an LTQFT instrument. Table 2 shows the characterization of the proteins coming out from the FT/MS. Beside differences in PIP composition we observed that the α- and β-subunits, which compose the 20S part of the proteasome were not pulled down from the non-irradiated sample. In contrary, all the α- and β-subunits were precipitated from the irradiated samples with high percentage of sequence coverage ranging from 30 to 70%. The proteasome is a highly dynamic structure with the 19S caps dissociating from and reassembling with the 20S core in an ATP-dependent fashion [1]. In contrary to Babbit et al. [1], our current working hypothesis is that ATP is required for 26S proteasome assembly and that in the presence of the non-hydrolysable form of ATP (ATPγS), 19S and 20S particles dissociate passively and ATP-independent but cannot be reassembled. This is in agreement with published data [2]. We interpret our results in a way that radiation interferes with the disassembling of 26S proteasomes, which stabilizes the 26S proteasome in a less active/inactive but intact state.

Table 2. List of proteins detected in presence of ATPγS in non-irradiated and irradiated samples. Data were analyzed with an FT/MS instrument.

	PC3 NON IRRADIATED	**PC3 ATPgS IRRADIATED**
DNA repair	UV excision repair protein RAD23 homolog B	UV excision repair protein RAD23 homolog B
Metabolism	Polyadenylate-binding protein 1	myristoylated alanine-rich protein kinase C substr
	Protein disulfide-isomerase A4	tyrosine 3-monooxygenase/tryptophan 5-monooxygenase
	Calreticulin	tyrosine 3/tryptophan 5 -monooxygenase activation protein
	Protein kinase C substrate	phosphoglycerate mutase 2 (muscle)
	Transferrin receptor (P90, CD71)	lactate dehydrogenase A
	Elongation factor 2	peptidylprolyl isomerase A
	Transglutaminase 2	glyceraldehyde-3-phosphate dehydrogenase
	Elongation factor 2	protein disulfide isomerase-associated 3 precursor
	C-1-tetrahydrofolate synthase, cytoplasmic	pyruvate kinase, muscle isoform 2
	Adenylyl cyclase-associated	
	Protein disulfide-isomerase	
	Glucose-6-phosphate isomerase	
	Peptidyl-prolyl cis-trans isomerase	
	Phosphoglycerate kinase	
	Elongation factor 1-alpha	
	Alpha-enolase	
	Glyceraldehyde 3-phosphate dehydrogenase	
	EIF-2A	
	Alpha-enolase	
	translocase of outer mitochondrial membrane 34	
	lactate dehydrogenase A and B	
	protein disulfide isomerase-associated 3 precursor	
	pyruvate kinase, muscle isoform 1	
	Peptidyl-prolyl cis-trans isomerase	
	M2-type pyruvate kinase	
	Glucose-6-phosphate isomerase	
	mitochondrial malate dehydrogenase precursor	
Translation	Bifunctional aminoacyl-tRNA	eukaryotic translation elongation factor 1 alpha 2
Transcr.	AHNAK nucleoprotein isoform 1	
	Eukaryotic initiation factor 4A-I	
	Eukaryotic translation initiation factor 4A1	
	EIF-2A	
	Elongation factor 1-gamma;	
	ribosomal protein L5	

	ribosomal protein P0	
	guanine nucleotide-binding protein, beta-1 subunit	
Cell signaling	Chaperonin containing TCP1, subunit 5	lactotransferrin
	Stress-induced-phosphoprotein	heat shock 70kDa protein 5
	Serine/threonine-protein phosphatase	heat shock 70kDa protein 8 isoform 1
	Heterogeneous nuclear ribonucleoprotein K	stress-induced-phosphoprotein 1
	T-complex protein 1 subunit alpha	glyceraldehyde-3-phosphate dehydrogenase
	60 kDa heat shock protein	
	HSPA5 protein	
	Heat shock 70kDa protein 8 isoform 1 variant	
	Heat shock protein HSP 90-beta	
	Heat shock 70 kDa protein 4	
	Hypoxia up-regulated protei	
	Clathrin heavy chain 1	
	T-complex protein 1 subunit beta	
	T-complex protein 1 subunit delta	
	adhesion regulating molecule 1 precursor	
Others	Myosin-9	filamin A, alpha isoform 1
	Filamin A	myosin, heavy polypeptide 9, non-muscle
	Vinculin	clathrin heavy chain 1
	Integrin beta-1	vinculin isoform VCL
	Endoplasmin	actinin, alpha 1
	Moesin	alpha 1 globin
	Alpha-actinin-1	beta globin
	Exportin-2	moesin
	L-plastin	apolipoprotein A-I preproprotein
	Annexin A6	annexin VI isoform 1
	filamin B, beta (actin binding protein 278)	peroxiredoxin 1
	dynein, cytoplasmic, heavy polypeptide 1	annexin I
	Beta 5-tubulin	thioredoxin-like 1
	Tubulin alpha-1A chain	annexin A2 isoform 1
	Actin, cytoplasmic 2	annexin A11
	thioredoxin-like 1	actin, gamma 1 propeptide
	annexin A2 isoform 1	
	annexin A11	
	clathrin heavy chain 1	
	Fascin	
26S	***19S Rpt***	***19S Rpt***
	Rpt2 PSMC 1	Rpt1 ATPase subunit 2 PSMC2
	Rpt3 PSMC4	Rpt2 ATPase subunit 1 PSMC1
	Rpt4 26S ATPase subunit 6 PSMC 6	Rpt3 PSMC4, transcript variant 1

	Rpt5 PSMC 3	Rpt4 ATPase subunit 6
	ATPase sub 5 PSMC 5	Rpt5 ATPase subunit 3
	26S ATPase subunit 5 PSMD 5	Proteasome 26S ATPase subunit 4
		proteasome 26S ATPase subunit 5 PSMD5
	19S Rpn	***19S Rpn***
	Rpn1 PSMD 2	Rpn1 non-ATPase subunit 2 PSMD 2
	Rpn2 PSMD 1	Rpn2 non-ATPase subunit 1 PSMD 1
	Rpn3 PSMD 3	Rpn5 non-ATPase subunit 12 PSMD12
	Rpn5 PSMD 12	Rpn6 non-ATPase subunit 11 PSMD11
	Rpn6 non-ATPase subunit 11 PSMD 11	Rpn8 non-ATPase subunit 7 PSMD 7
	Rpn7 non-ATPase reg. subu 6 PSMD 6	Rpn9 non-ATPase subunit 13 isoform 2
	Rpn8 non-ATPase reg. sub 7 PSMD7	Rpn10 non-ATPase subunit 4
	Rpn9 non-ATPase sub 13 isof 1 PSMD13	Rpn11 non-ATPase regulatory subunit 14
	Rpn10 26S non-ATPase subunit 4	Rpn12 non-ATPase subunit 8 PSMD 8
	Rpn11 non-ATPase reg. subunit 14	
	Rpn12 PSMD 8	
	20S	***20S***
		proteasome alpha 1 subunit isoform 1
		proteasome alpha 2 subunit 20S
		proteasome alpha 3 subunit isoform 1
		proteasome alpha 4 subunit isoform 1
		proteasome alpha 5 subunit
		proteasome alpha 6 subunit
		proteasome alpha 7 subunit
		proteasome beta 1 subunit
		proteasome beta 2 subunit
		proteasome beta 3 subunit
		proteasome beta 4 subunit
		proteasome beta 5 subunit
		proteasome beta 6 subunit
		proteasome beta 7 subunit proprotein
		proteasome beta 9 subunit isoform 2 proprotein
		proteasome beta 10 subunit proprotein
	Others	***Others***
	ubiquitin-binding protein homolog	ubiquitin C
	Ubiquitin-like modifier-activating enzyme 1	ubiquitin C-terminal hydrolase UCH37
	26S protease regulatory sub 6A/TAT-binding protein 1	proteasome activator subunit 1 isoform 2
	26S proteasome-associated pad1 homolog	26S proteasome-associated pad1 homolog
	ubiquitin specific protease 14 isoform a	ubiquitin specific protease 14 isoform a

An important control experiment to standardize proteasome function readouts after irradiation was to test, whether the activity of this protease changes during the cell cycle and if this coincides with changes in its susceptibility to radiation.
To test this, we synchronized PC3 cells using aphidocolin, a drug that blocks the cell cycle in the G1/early S phase. We studied the 26S proteasome activity at 3, 6, 12, 24 hours after restarting the cell cycle and in parallel the cell cycle distribution and compared it to non-treated cells. Using a substrate for the chymotryptic activity of the proteasome, we observed a drop of activity at 12 hours and its recovery at 24h (when cells started to redistribute). Cell cycle analysis showed that the cells with the lowest proteasome activity were in the G2/M phase and some of them were entering G1. Interestingly, the extent of inhibition was the same as the one seen after irradiation, suggesting the possibility that both phenomena employ the same pathways (Fig. 4). We are currently investigating and characterizing the proteins/kinases that may alter 26S proteasome activity through posttranslational modifications (in particular phosphorylation) and during the cell cycle and in response to radiation.

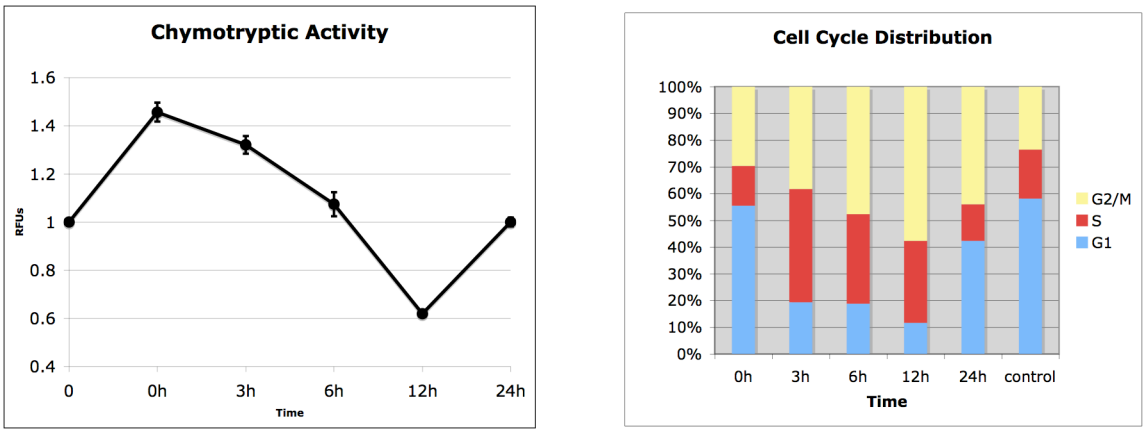

Figure 4. Chymotrypsin-like activity in PC3 in different phase of their cell cycle (left). Corresponding cell cycle distribution (right).

Beside the regulation of the 26S proteasome at the posttranslational level, we also planned to investigate the role of transcription in proteasome recovery and possible changes in proteasome composition with time (aim 1.d). In order to do that we proposed to irradiate cells (compare them with non-irradiated cells) and treat them with a polymerase inhibitor to block the transcription (DBR). Cells were treated with DBR 10 minutes after being exposed to a dose of radiation of 10Gy. The extracts were made at different time points measuring the chymotrypsin-like 26S proteasome activity by a fluorogenic assay. Our data so far suggest that transcription is not required for radiation-induced inhibition of 26S proteasome activity (figure 5), which is consistent with the immediate nature of radiation-induced inhibition.

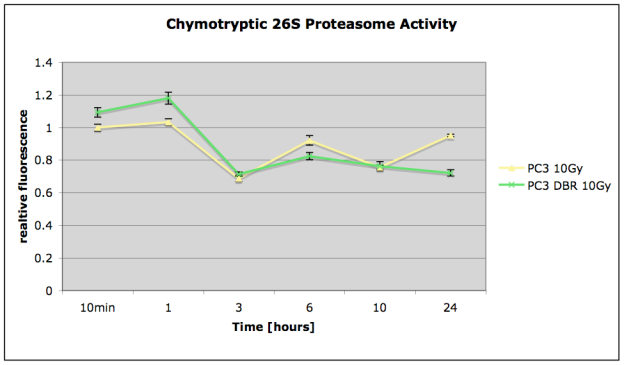

Figure 5. PC3 cells treated with DBR, an inhibitor of polymerase II. Proteins were extracted at different time points and the chymotrypsin-like 26S proteasome activity was measured.

Key Research Accomplishment:

1. Study of the 26S subunits profile with proteomics tools using the biotin-tagged Rpn11 subunit
2. Establishment of an additional prostate cancer cell line transfected with the Rpn11 biotin vector to prove the robustness of the method.
3. Characterization of proteins associate to the proteasome (PIPs) by SDS-PAGE coupled with mass spectrometry (FT/MS) and 2D-LC/MSMS
4. Identification of proteins differently associated with the proteasome in irradiated cells versus non-irradiated cells
5. Demonstration that ATP alters the response of 26S proteasomes to radiation.
6. Establishment of a protocol for studying the phosphorylation status of a protein by mass spectrometry
7. Excluding transcription as the mechanism of radiation-induced 26S proteasome inhibition
8. Discovery that 26S proteasome activity is regulated during the cell cycle

Reportable outcomes:

Poster presentation, William H. McBride, James Brush, Keisuke Iwamoto, Kwanghee Kim, Frank Pajonk, Milena Pervan. *Irradiation alters protein expression through direct effects on the 26S proteasome,* AACR, Los Angeles, 2007

Poster presentation, William H. McBride, Frank Pajonk, Kei Iwamoto, James Brush, Kwanghee Kim, *Radiation modifies cell signaling through altering proteasome structure and function,* International Wolfsbergmeeting, 2007

Oral and *poster* presentation at the Radiation Research Society (RRS) 54th Annual Meeting, 21-24 September, Boston: Lorenza Della Donna, Chann Lagadec, Erina Vlashi, Kwanghee Kim, Tyson McDonald, Julian Whitelegge, William H. McBride and Frank Pajonk *Radiation-induced posttranslational modification and expression of proteasome subunits, 2008*

SIT Travel Award to Lorenza Della Donna from the Radiation Research Society (RRS), 54th Annual Meeting, 21-24 September, Boston, 2008

Invited Lecture, Lorenza Della Donna, Biomedical Physics Interdepartmental Graduate Program, *Proteomics as a solution to complex problems, 2008*

Poster presentation at the AACR 10th Annual Meeting (Denver, CO) Lorenza Della Donna, Erina Vlashi, Chann Lagadec, Julian Whitelegge, Puneet Souda, Polin Nikolay, Malcom Mattes, William McBride and Frank Pajonk. *Quantitative proteomic analysis of radiation induced posttranslational modifications of the 26S proteasome, 2009*

Erina Vlashi, Kwanghee Kim, Chann Lagadec, Lorenza Della Donna, J. Tyson McDonald, Mansoureh Eghbali, James W. Sayre, Encrico Stefani, William McBride, and Frank Pajonk *In-vivo imaging, tracking, and targeting of cancer stem cells*, JNCI, 2009 (in press)

Conclusion:

Our results so far have shown that mass spectrometry tools and protocols developed during this year are powerful tools to detect changes in 26S proteasome composition and posttranslational modification upon irradiation. The observation that radiation stabilized the 19S-20S complexes, is an important step forward to understand the mechanisms underlying radiation-induced inhibition of this protease. Our data showing that the key regulator of cell cycle progression itself is regulated during the cell cycle is a seminal discovery, which will broaden our understanding of how cells replicate.

References:

1. Babbitt, S. E. et al. ATP hydrolysis-dependent disassembly of the 26S proteasome is part of the catalytic cycle. Cell 121, 553-65 (2005).
2. Liu, C. W. et al. ATP binding and ATP hydrolysis play distinct roles in the function of 26S proteasome. Mol Cell 24, 39-50 (2006).

Appendix:

Preprint, Vlashi et al., JNCI, 2009

	JNCI	djn509	PA
	JOURNAL NAME	Art. No.	CE Code

ARTICLE

In Vivo Imaging, Tracking, and Targeting of Cancer Stem Cells

Erina Vlashi, Kwanghee Kim, Chann Lagadec, Lorenza Della Donna, J. Tyson McDonald, Mansoureh Eghbali, James W. Sayre, Encrico Stefani, William McBride, Frank Pajonk

Background There is increasing evidence that solid cancers contain cancer-initiating cells (CICs) that are capable of regenerating a tumor that has been surgically removed and/or treated with chemotherapy and/or radiation therapy. Currently, cell surface markers, like CD133 or CD44, are used to identify CICs in vitro; however, these markers cannot be used to identify and track CICs in vivo. The 26S proteasome is the main regulator of many processes within a proliferating cell, and its activity may be altered depending on the phenotype of a cell.

Methods Human glioma and breast cancer cells were engineered to stably express ZsGreen fused to the carboxyl-terminal degron of ornithine decarboxylase, resulting in a fluorescent fusion protein that accumulates in cells in the absence of 26S proteasome activity; activities of individual proteases were monitored in a plate reader by detecting the cleavage of fluorogenic peptide substrates. Proteasome subunit expression in cells expressing the fusion protein was assessed by quantitative reverse transcription—polymerase chain reaction, and the stem cell phenotype of CICs was assessed by a sphere formation assay, by immunohistochemical staining for known stem cell markers in vitro, and by analyzing their tumorigenicity in vivo. CICs were tracked by in vivo fluorescence imaging after radiation treatment of tumor-bearing mice and targeted specifically via a thymidine kinase–degron fusion construct. All *P* values were derived from two-sided tests.

Results Cancer cells grown as sphere cultures in conditions, which enrich for cancer stem cells (CSCs), had decreased proteasome activity relative to the respective monolayers (percent decrease in chymotryptic-like activity of sphere cultures relative to monolayers—U87MG: 26.64%, 95% confidence interval [CI] = 10.19 to 43.10, GL261, 52.91%, 95% CI = 28.38 to 77.43). The cancer cells with low proteasome activity can thus be monitored in vitro and in vivo by the accumulation of a fluorescent protein (ZsGreen) fused to a degron that targets it for 26S proteasome degradation. In vitro, ZsGreen-positive cells had increased sphere-forming capacity, expressed CSC markers, and lacked differentiation markers compared with ZsGreen-negative cells. In vivo, ZsGreen-positive cells were approximately 100-fold more tumorigenic than ZsGreen-negative cells when injected into nude mice (ZsGreen positive, 30 mice per group; ZsGreen negative, 31 mice per group), and the number of CICs in tumors increased after 72 hours post radiation treatment. CICs were selectively targeted via a proteasome-dependent suicide gene, and their elimination in vivo led to tumor regression.

Conclusion Our results demonstrate that reduced 26S proteasome activity is a general feature of CICs that can easily be exploited to identify, track, and target them in vitro and in vivo.

J Natl Cancer Inst 2009;101:1–10

Cancer cell propagation in vivo has been explained by the "stochastic model" (1,2), which claims that every cancer cell in a tumor can ultimately acquire a capacity for self-renewal and multilineage potency so that it can repopulate an entire tumor. The stochastic model of cancer has long been regarded as the only working model of cancer organization, largely because until recently it has not

Affiliations of authors: Division of Molecular and Cellular Oncology, Department of Radiation Oncology (EV, KK, CL, LDD, JTM, WM, FP), Department of Anesthesiology (ME, ES), David Geffen School of Medicine at University of California, Los Angeles, Biostatistics and Radiological Sciences, School of Public Health (JWS), University of California, Los Angeles, Johnson Comprehensive Cancer Center (WM, FP), University of California, Los Angeles.

Correspondence to: Frank Pajonk, Division of Molecular and Cellular Oncology, Department of Radiation Oncology, David Geffen School of Medicine at University of California, Los Angeles, 10833 Le Conte Ave, Los Angeles, CA 90095-1714 (e-mail: fpajonk@mednet.ucla.edu).

See "Funding" and "Notes" following "References."

DOI: 10.1093/jnci/djn509

CONTEXT AND CAVEATS

Prior knowledge

The interaction of the protein netrin-1 with dependence receptors acts to regulate the cell's commitment to apoptosis. It had been suggested that the proapoptotic activity of unliganded dependence receptors is a mechanism for checking the proliferation of tumor cells and that overexpression of their ligands could be a means by which tumor cells escaped this control.

Study design

Netrin-1 expression was assessed in a panel of non–small cell lung cancers (NSCLCs) and human lung cancer cell lines. The netrin-1 activity in cancer cells was modulated by specifically targeting netrin-1 expression or function, and the effects on cell death and lung tumor growth in mice were assessed. The dependence receptors for netrin-1 were identified by transfecting cells with dominant-negative mutant candidate receptors.

Contribution

This study confirmed a role for the interaction of netrin-1 with a cognate dependence receptor in the regulation of cancer cell death and lung tumor growth in vivo. High levels of netrin-1 in human NSCLC tumors suggested a possible role for the interaction of netrin-1 with dependence receptors in human lung cancer.

Implications

Alterations in signaling by netrin-1 dependence receptors may play an important role in the progression of human lung cancer.

Limitations

The functional importance of netrin-1 action in human cancer, as opposed to model systems, and the usefulness for therapeutic purposes of targeting signaling by dependence receptors remain to be determined.

From the Editors

been possible to prospectively isolate the very small population of cancer stem cells (CSCs) from the bulk of an unselected tumor cell population for characterization. In addition, working with unselected cell populations is inexpensive and experimental responses of the bulk of these cells can be easily used as a rationale for pharmaceutical approaches against cancer. Unfortunately, and despite an enormous effort, these approaches based on the behavior of unselected cell populations, even those termed targeted cancer therapies, have not yet resulted in cancer cures.

An alternative view of cancer cell propagation that is now supported by an increasing body of experimental evidence is the hierarchical model (3). It assumes that most, if not all, solid cancers are characterized by a hierarchical organization in which there are small populations of cancer stem cells (CSCs)/cancer-initiating cells (CICs) that are capable of repopulating an entire tumor, but whose progeny lacks this ability (1). Although this model has long been postulated, it has only recently become possible to provide supporting experimental evidence because of technological advances, such as the availability of sophisticated fluorescence-activated cells sorting (FACS) instruments, which are capable of efficiently isolating viable populations of rare cells from the bulk of tumor cells based on their expression of several cell surface markers. An increasing number of cell surface markers have been used to distinguish CSCs and CICs from the bulk of the tumor cells and to demonstrate their self-renewal capacity, multilineage potency, lack of expression of differentiation markers, and increased tumorigenicity when injected into immune-deficient mice (4–10). CSCs/CICs identified in this way have been shown to be relatively resistant to conventional anticancer therapies, such as chemotherapy and/or radiation therapy (11–13), and there is now strong evidence to suggest that a successful cancer treatment strategy will have to be based on the elimination of this cell population via novel therapeutic approaches. Thus, although it is becoming increasingly important to identify, track, and target CSCs/CICs in vivo, available markers are not very suitable for the purpose. A reliable system that would allow identification and tracking of CSCs/CICs would be an invaluable tool to study the effects of established and novel therapies on CSCs/CICs, but one that requires identification of cellular factors specific to this population.

The 26S proteasome is a multicatalytic protease complex with at least three distinct kinds of proteolytic activities—chymotrypsin like, trypsin like, and caspase like. It accounts for almost 1% of total protein expressed in eukaryotic cells and is a key regulator of many cellular functions, including cell cycle control, DNA repair, cell death, and survival (14). Its inhibition causes apoptosis and sensitization of cells to chemotherapeutic agents (15) and ionizing radiation (16,17). Furthermore, conventional anticancer therapies, for example, ionizing radiation (18), chemotherapeutic drugs (19,20), and hyperthermia (21), inhibit the proteasome, suggesting that their anticancer activity may be mediated by effects on this protein complex.

A proteasome inhibitor, bortezomib, is in clinical use for patients suffering from multiple myeloma or mantle cell lymphoma (22). However, despite its excellent preclinical efficacy in animal models of other cancers, bortezomib failed to demonstrate antitumor activity as a single agent in patients with solid cancers in clinical trials, suggesting that CICs might not be affected by proteasome inhibition (23–27). The results of these clinical studies prompted us to investigate proteasome activity and subunit expression in CICs of solid cancers relative to that in monolayer cultures and to examine whether proteasome activity is a useful marker for CICs. To monitor proteasome activity in living cells, we generated cancer cell lines that stably expressed a fusion protein consisting of a fluorescent protein fused to a degron, a sequence that targets the fusion protein for destruction by the proteasome. We also generated cancer cell lines expressing the degron fused to the suicide gene thymidine kinase (TK) to specifically investigate the effect of eliminating cells with low proteasome activity on sphere-forming capacity and self-renewal in vitro and tumor growth in vivo.

Materials and Methods

Cell Culture

Human U87MG glioma cell line was a kind gift from Dr P. Michel (Department of Pathology, University of California, Los Angeles, Los Angeles, CA). Murine GL261 glioma and 67NR breast cancer cell lines were a kind gift from Dr Sandra DeMaria (Department of Pathology, New York University School of Medicine, New York, NY). Human U343 and MCF-7 breast cancer cell lines were purchased from American Type Culture Collection (Manassas, VA).

All cells were cultured in log-growth phase in DMEM (Invitrogen, Carlsbad, CA) (supplemented with 10% FBS [Sigma, St Louis, MO] and penicillin/streptomycin cocktail [Sigma]) and were grown in a humidified incubator at 37°C at 5% CO_2. To obtain CICs, MCF-7, 67NR, U87MG, U343, and GL261 cells were seeded into selection media (DMEM/F12, 0.4% BSA [Sigma], 10 mL/500 mL B27 [Invitrogen], 5 μg/mL bovine insulin [Sigma], 4 μg/mL heparin [Sigma], 20 ng/mL fibroblast growth factor 2 [bFGF, Sigma], and 20 ng/mL epidermal growth factor [EGF, Sigma]) at a density of 1000 cells per mL. Under these conditions, only CICs and early progenitor cells survive and proliferate, whereas differentiated cells die (28).

Generation of Stable Cell Lines Expressing ZsGreen-cODC and TK-ZsGreen-cODC Fusion Proteins Using Retroviral Transduction

Proteasomal degradation of most proteins depends on their ubiquitination. However, a small number of proteins such as ornithine decarboxylase (ODC) contain amino acid sequences that are directly recognized by the proteasome, which leads to the immediate destruction of the proteins that contain them. Viral expression vectors in which the carboxyl terminus of the murine ornithine decarboxylase (cODC) degron was fused to reporter proteins were constructed as follows. ZsGreen-cODC: The degron from the carboxyl-terminal 37 amino acids of ODC fused to ZsGreen (ZsGreen-cODC) was digested with *Bgl*II and *Not*I from pZsProsensor-1 (BD Biosciences, San Jose, CA) and cloned into the *Bam*HI and *Eco*RI sites of the retroviral vector pQCXIN (BD Biosciences) using the *Not*I-*Eco*RI DNA oligonucleotide adaptor (EZCLONE Systems, New Orleans, LA). TK-ZsGreen-cODC: ZsGreen-cODC was amplified from pZsProsensor-1 and cloned into the *Bam*HI and *Eco*RI sites of pQCXIN vector (pQCXIN-BamH1 -ZsGreen-ODC). The sequence of TK was amplified from pORF-HSVtk expression vector (InvivoGen, San Diego, CA) and cloned into pQCXINBamH1-ZsGreen-cODC using the *Not*I and *Bam*HI sites (pQCXIN/TK-ZsGreen-ODC). pQCXIN/ZsGreen-cODC or pQCXIN/TK-ZsGreen-cODC was transfected into GP2-293 pantropic retroviral packaging cells (BD Biosciences). The retrovirus collected from the supernatant of the packaging cells was used to infect the different cell lines. Stable transfectants were selected with G418 (Invitrogen). The accumulation of ZsGreen-cODC protein was monitored by flow cytometry (FL-1 channel). To determine that the cells not accumulating the ZsGreen-cODC protein still contained the expression vector, the cells were incubated with 50 μM of the proteasome inhibitor MG-132 (Calbiochem, San Diego, CA) for 4 hours and the accumulation of the ZsGreen-cODC protein due to proteasome inhibition was analyzed by flow cytometry.

Primary Sphere Formation Assay

ZsGreen-cODC–expressing U87MG cells were grown in selection media as sphere cultures (primary spheres) and were sorted into ZsGreen-negative and -positive populations by FACS. Cells were defined as "ZsGreen positive" if the fluorescence in the FL-1 channel exceeded the fluorescence of nontransfected control cells by at least three orders of magnitude. The two cell populations were plated in selection media into 96-well plates, ranging from 1 to 100 cells per well. Growth factors, EGF and bFGF, were added every 3 days, and the cells were allowed to form spheres (secondary spheres) for 7–10 days. The number of spheres formed per well was then counted and expressed as a percentage of the initial number of cells plated. Four independent experiments were performed.

Proteasome Function Assays

Chymotryptic, tryptic, and caspase proteasome activities were measured as described previously (29) with a few minor modifications. MCF-7, 67NR, U87MG, U343, and GL261 cells were washed with PBS and pelleted by centrifugation. Glass beads and homogenization buffer (25 mM Tris [pH 7.5], 100 mM NaCl, 5 mM ATP, 0.2% [vol/vol] Nonidet P-40 and 20% glycerol) were added to the cells, and the mixtures were vortexed for 1 minute. Beads and cell debris were removed by centrifugation at 4°C. Protein concentration in the resulting crude cellular extracts was determined by the Micro BCA protocol (Pierce, Rockford, IL) with BSA (Sigma) as standard. To measure 26S proteasome activity, 100 μg of protein from crude cellular extracts of each sample was diluted with buffer I (50 mM Tris [pH 7.4], 2 mM DTT, 5 mM $MgCl_2$, 2 mM ATP) to a final volume of 1 mL (assayed in quadruplicate). The fluorogenic proteasome substrates Suc-LLVY-AMC (chymotryptic substrate; Biomol International, Plymouth Meeting, PA), Z-ARR-AMC (tryptic substrate; Calbiochem), and Z-LLE-AMC (caspase-like substrate; Biomol International) were dissolved in DMSO and added to a final concentration of 80 μM in 1% DMSO. Proteolytic activities were continuously monitored by measuring the release of the fluorescent group, 7-amido-4-methylcoumarin (AMC), with the use of a fluorescence plate reader (Spectramax M5, Molecular Devices, Sunnyvale, CA) at 37°C, at excitation and emission wavelengths of 380 and 460 nm, respectively.

Luminescence ATP Detection Assay

Single-cell suspensions derived from U87MG-ZsGreen-cODC monolayer cultures (1000 cells) or 3-day-old primary sphere cultures were plated into 96-well plates of DMEM or DMEM/F12 selection medium (100 μL per well). The proteasome inhibitor PS341 (kind gift of Julian Adams, Millennium Pharmaceuticals, Cambridge, MA) was added at the indicated concentrations. After 5 days of incubation, 40 μL of ATP-lite substrate (Perkin-Elmer, Waltham, MA) was added to each well and luminescence was measured immediately using a fluorescence plate reader (Spectramax M5).

Quantitative Reverse Transcription–Polymerase Chain Reaction

Total RNA was isolated from U87MG monolayer cells and from sorted ZsGreen-cODC–positive and –negative cells using TRIZOL Reagent (Invitrogen). Complementary DNA (cDNA) synthesis was carried out using TaqMan Reverse Transcription Reagents (Applied Biosystems, Foster City, CA). Quantitative polymerase chain reaction (PCR) of proteasome subunit cDNAs was performed in an iQ5 Real-Time PCR Detection System (Bio-Rad, Hercules, CA) using the 2× iQ SYBR Green Supermix (Bio-Rad). C_t for each gene was determined after normalization to GAPDH,

and $\Delta\Delta C_t$ was calculated relative to the designated reference sample. Gene expression values were then set equal to $2^{-\Delta\Delta Ct}$ as described by the iQ5 Optical System Software (Bio-Rad). All PCR primers were synthesized by Invitrogen and designed to amplify human *GAPDH* and the human proteasome subunits *Lmp2*, *Y*, *Mecl1*, *Z*, *Lmp7*, *X*, *11S PA28alpha*, *11S PA28beta*, *19S ATPase PSMC1*, and *19S non-ATPase PSMD4* (all primer sequences are provided in the Supplementary Methods, available online).

Mice

Nude (nu/nu), 6- to 8-week-old female mice originally from The Jackson Laboratories (Bar Harbor, ME) were rederived, bred, and maintained in a Defined Flora environment in the Association for the Assessment and Accreditation of Laboratory Animal Care International–accredited animal facilities of the Department of Radiation Oncology, University of California, Los Angeles (Los Angeles, CA) in accordance with all local and national guidelines for the care of animals. We used 74 mice for the in vivo experiments: 61 mice were used for the tumorgenicity experiments, 10 mice were implanted with U87-TK-ZsGreen-ODC tumors, and three mice were used to analyze the effect of fractionated radiation on U87MG-ZsGreen-ODC tumors.

Tumor Xenotransplantation and Tumorigenicity

U87MG-ZsGreen–high or U87MG-ZsGreen–negative cells derived from 5- to 6-day-old spheres and sorted by FACS were injected subcutaneously into both thighs of nude mice (10^6, 10^5, 10^4, 10^3, or 10^2 cells per inoculum), and each tumor was considered as the unit of analysis. The number of tumors used for each group is summarized in Table 1. Tumor growth was monitored on a weekly basis, and the mice were killed by CO_2 asphyxiation when the tumor size reached the protocol guidelines requiring euthanasia (1.3 cm in diameter).

Fractionated Radiation

Subcutaneous tumors (average diameter of 1 cm) generated from implanting 1×10^6 cells derived from unselected U87MG-ZsGreen-cODC monolayers into the thighs of nude mice were irradiated with 3 Gy for 5 consecutive days, using a cobalt-60 source (dose rate 0.6 Gy/min). The thighs of anesthetized mice bearing the tumor were placed in a 5- × 5-cm radiation field of the cobalt-60 source, whereas the rest of the body was shielded. The mice were anesthetized at different time points after irradiation and imaged for the macroscopic presence of ZsGreen-positive cells in the tumors using the Maestro In-Vivo Imaging System (Cambridge Research & Instrumentation, Woburn, MA).

Table 1. Enhanced tumor formation by cells with low levels of 26S proteasome*

	Fraction (%) of injected mice that developed tumors		
No. of cells injected	Injected with ZsGreen-high cells	Injected with ZsGreen-negative cells	Injected with ZsGreen-negative cells, and excluding ZsGreen-positive tumors†
10^2	1/4 (25%)	0/3	0/3
10^3	8/11 (73%)	1/4 (25%)	0/3
10^4	10/11 (91%)	5/9 (56%)	2/6 (33%)
10^5	4/4 (100%)	7/10 (70%)	4/7 (57%)
10^6	—	4/5 (80%)	2/3 (67%)

* The ZsGreen protein was fused to the murine ornithine decarboxylase degron and its accumulation was thus an indicator of low proteasome activity.

† When the tumors that arose from injections with ZsGreen-negative cells resulted in macroscopically green tumors, they were excluded from the total number of tumors formed from the ZsGreen-negative population.

Immunocytochemistry

Spheres from U87MG-ZsGreen-cODC cells that were 5–6 days old were transferred onto glass slides by cytocentrifugation (Cytospin; Shandon Elliot, London, UK) and fixed with 4% formaldehyde. The cells were incubated in permeabilization buffer (10% saponin, 0.5% BSA, in PBS) for 10 minutes, followed by incubation with the following primary antibodies for 30 minutes at room temperature: rabbit anti-human nestin (1:500) (Abcam, Cambridge, MA), rabbit anti-human GFAP (1:1000) (Abcam), mouse anti-human TUJ-1 (1:1000) (Abcam), mouse anti-human Sox2 (10 μg/mL) (R&D Systems, Minneapolis, MN), or mouse anti-human Musashi-1 (10 μg/mL) (R&D Systems). For staining with the mouse anti-human 19S regulator non-ATPase subunit Rpn2 (1:200) (Biomol International), the slides were first incubated with 5% goat serum in PBS /Triton to block nonspecific antibody binding, and then with the primary antibody overnight at 4°C. The secondary antibodies (TRITC -conjugated goat anti-rabbit IgG [1:200], and TRITC-conjugated goat anti-mouse Fab [1:80], both from Sigma) were diluted in PBS /1% BSA/0.5% saponin and incubated with the cells for 1 hour. Hoechst 33342 (5 μg/mL; Invitrogen) solution was added for nuclear staining. The slides were visualized with an Olympus IX71 inverted fluorescent microscope.

Immunohistochemistry

Tumors were removed from killed mice and fixed in buffered formalin. The tissue was then embedded in paraffin and cut into 4-μm sections. The tissue sections were deparaffinized in xylene (2 × 5 minutes) and rehydrated in a graded series of ethanol solutions (100%, 90%, 75%, 50%, and 25%) for 5 minutes each, followed by a final rinse in PBS. Antigen retrieval was performed by incubating the sections with CAREZYME I-Trypsin solution (BioCare Medical, Concord, CA). The sections were incubated with 10% goat serum in PBS to block nonspecific binding. The primary antibodies, rabbit anti-human Ki67 (1:100) (Abcam), and mouse anti-human CD31 (10 μg/mL) (Abcam) were diluted in 1% BSA/PBS and incubated with the sections overnight at 4°C. TRITC-conjugated secondary antibodies (TRITC-conjugated goat anti-rabbit IgG [1:80], and TRITC-conjugated goat anti-mouse Fab [1:400], both from Sigma) diluted in 1% BSA/PBS were added for 1 hour. Hoechst 33342 was added for 10 minutes at room temperature. The sections were visualized using an Olympus IX71 inverted fluorescent microscope.

Statistical Analysis

All results are expressed as mean values with 95% confidence intervals. For the proteasome activity assays, normal distributions of the data were confirmed using a Kolmogorov–Smirnov test. All statistical

comparisons used a two-sided paired Student *t* test. The test was applied to normalized data to compensate for the variance of measurements between biologically independent replicates of the same experiments. Statistical significance was defined as $P \leq .05$.

Results

Proteasome Activities of CICs in Breast Cancer and Glioma

We recently reported that sublethal doses of ionizing radiation increased the number of CICs in breast cancer (13) and sought to prevent this increase by blocking cell cycle progression using proteasome inhibitors. The approach was ineffective because CICs derived from mammospheres (data not shown) or glioma neurospheres were very resistant to proteasome inhibition (Supplementary Figure 1, A and B, available online). To monitor 26S proteasome activity in living cells, we stably transduced murine and human glioma and breast cancer cells lines with a fusion of a fluorescent protein, ZsGreen, and the degron from the cODC using retroviral vectors. The cODC is recognized by the 26S proteasome in an ubiquitin-independent manner (30), thus leading to immediate degradation of the ZsGreen fluorescent protein. Untreated monolayer cultures of U87MG exhibited low background fluorescence in more than 94% of the cells, but very few cells (<4%) displayed high levels of ZsGreen expression (Figure 1, A). Treatment of cultures with proteasome inhibitors, such as MG-132, caused 100% of cells to express ZsGreen (data not shown). Interestingly, primary spheres that are derived from U87MG cells under serum-free conditions and which are highly enriched for CICs (31,32) were greatly enriched for ZsGreen-positive cells (Figure 1, B), indicating that CICs may have low 26S proteasome activity.

To validate this observation, we performed fluorogenic proteasome function assays using monolayer and primary sphere cultures from U87MG human glioma and GL261 murine glioma cells (29). Chymotrypsin-like activity, the predominant activity of the 26S proteasome, as well as caspase-like activity were reduced in the sphere cultures, whereas the trypsin-like activity of U87MG cells was increased (percent decrease in proteasome activities of sphere cultures relative to monolayer cultures, mean of difference: chymotryptic-like activity, 26.64%, 95% CI = 10.19 to 43.10, $P = .02$, n = 3; trypsin-like activity, 39.46%, 95% CI = 88.18 to 9.266, $P = .08$, n = 4; caspase-like activity, 38.74%, 95% CI = 15.29 to 62.20, $P = .01$, n = 4; GL261: chymotryptic-like activity, 52.91%, 95% CI = 28.38 to 77.43, $P = .006$, n = 4; trypsin-like activity, 65.23%, 95% CI = 49.03 to 81.43, $P = .001$, n = 4; caspase-like activity, 52.88%, 95% CI = 18.22 to 124, $P = .09$, n = 3; Figure 1, C and D). Using the same fluorogenic peptide assays, reduced proteasome activity was further confirmed in U343 human glioma cells (proteasome activities of sphere cultures relative to the monolayer, mean of difference: chymotryptic-like activity, 37.74%, $P = .01$; trypsin-like activity, 26.25%, $P = .03$; caspase-like activity, 35.34%, $P = .04$; Supplementary Figure 1, C, available online), as well as in human and murine breast cancer cells, MCF-7 and 67NR (proteasome activities of sphere cultures

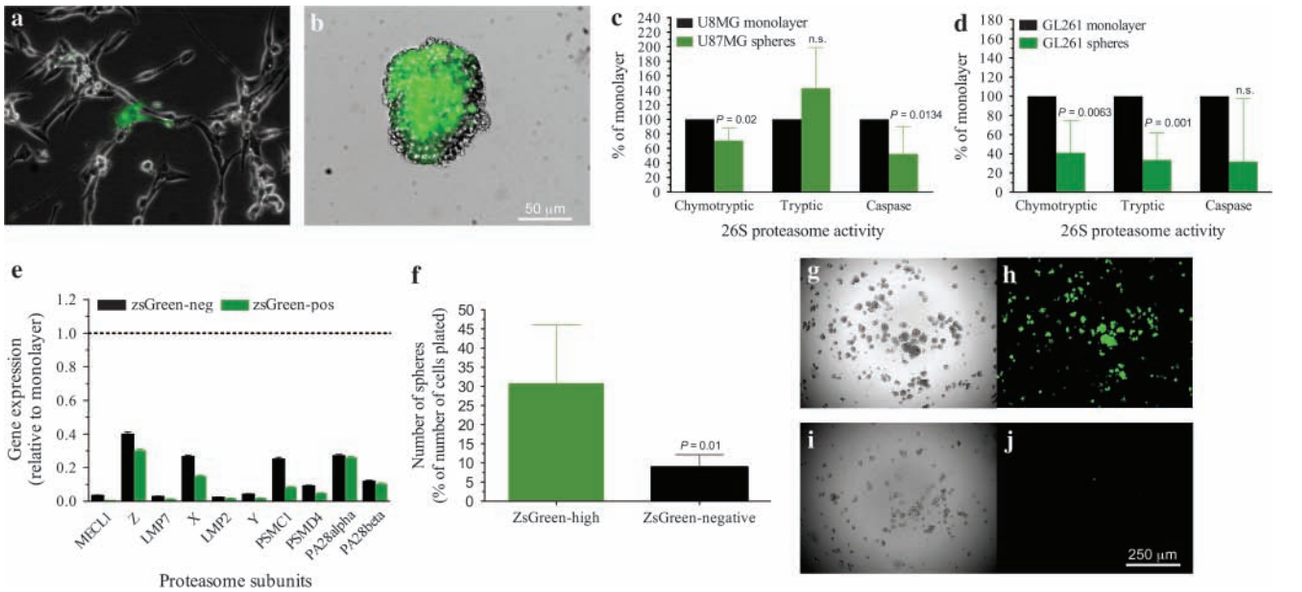

Figure 1. Characterization of cancer-initiating cells based on their proteasome activity. **A, B**) Frequency of cells in U87MG monolayer cultures (A) and U87MG-derived primary spheres (B) with accumulation of ZsGreen-cODC, and thus low proteasome activity. **C, D**) Proteasome activities of the 26S proteasome in U87MG (C) and GL261 (D) monolayer and sphere cultures. Means ± 95% confidence intervals (CIs) derived from three to four independent experiments (four replicates per experiment). The Kolmogorov–Smirnov test was used to confirm the normal distribution of the data, and the Student paired, two-tailed *t* tests were performed. **E**) Reverse transcription—polymerase chain reaction analysis of expression of mRNAs encoding proteasome components in ZsGreen-positive and ZsGreen-negative cells derived from spheres relative to expression in unselected monolayers (**dotted line**), three independent experiments. **F**) Number of spheres formed from the ZsGreen-high population vs the ZsGreen-negative population after sorting with flow cytometry into 96-well plates. Means ± 95% CIs from four independent experiments are shown. **G, H**) Secondary spheres derived from fluorescence-activated cells–sorted ZsGreen-high (G and H) and ZsGreen-negative cells (**I**, **J**). An image of bright field (**left**) and ZsGreen fluorescence (**right**) is shown for both populations.

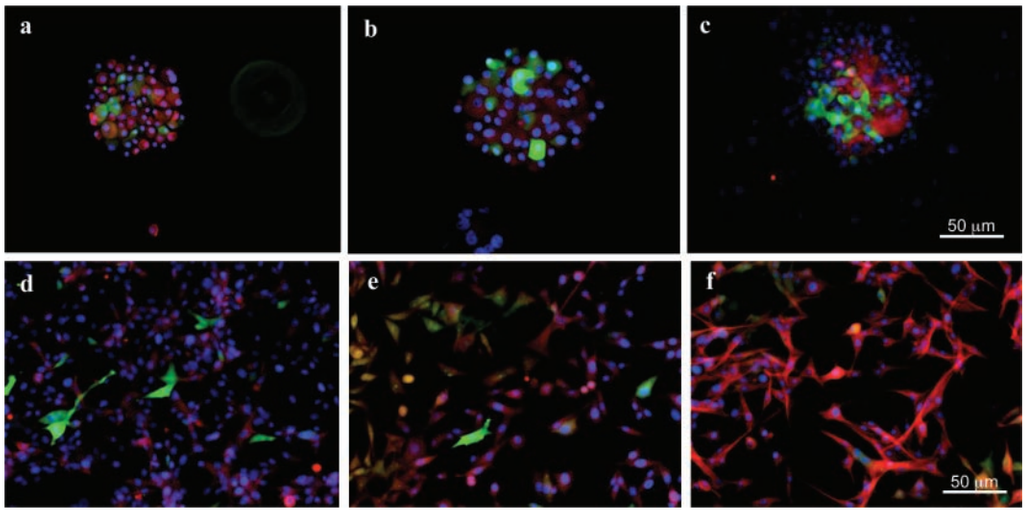

Figure 2. Cancer stem cell phenotype of cancer cells with low proteasome activity. **A–C**) Cytospins of U87MG-ZsGreen-cODC–derived neurospheres. ZsGreen-positive cells are positive for the stem cell marker nestin (**red**, A) but negative for the differentiation markers GFAP (red, B) and TUJ-1 staining of neuron-specific class III -tubulin (red, C). **D–F**) U87MG-ZsGreen-cODC–derived neurospheres differentiated in the presence of FBS . Cells lost expression of ZsGreen and nestin (red, D) but expressed the differentiation markers GFAP (red, E) and exhibited TUJ-1 staining of neuron-specific class III -tubulin (red, F). Counterstaining was performed with DAPI (**blue**).

relative to the monolayer, mean of difference—MCF-7: chymotryptic-like activity, 56.62%, $P = .1$; trypsin-like activity, 56.51%, $P = .02$; caspase-like activity, 36.92%, $P = .041$; 67NR: chymotryptic-like activity, 46.4%, $P = .004$; trypsin-like activity, 15.87%, $P = .008$; caspase-like activity, 55.45%, $P = .055$; Supplementary Figure 1, D and E, available online), indicating that reduced proteasome activity in CICs is a feature found across tumor entities of different species. Furthermore, quantitative reverse transcription—polymerase chain reaction revealed that several proteasome subunit mRNAs were decreased more than 100-fold in sphere cultures of CICs compared with cells in monolayer cultures (Figure 1, E). Confocal microscopy imaging for the Rpn2 subunit of the regulatory 19S cap of the 26S proteasome revealed a marked decrease in its expression in cells positive for ZsGreen (low proteasome activity), whereas cells lacking ZsGreen (high proteasome activity) expressed substantial levels of Rpn2 (Supplementary Figure 2, A–D, available online). Interestingly, a low 20S proteasome function has previously been reported for embryonic stem cells (33).

CICs, Proteasome Activity, and the CSC Phenotype

ZsGreen-high cells had a statistically significantly higher secondary sphere-forming capacity compared with the ZsGreen-negative population (average number of spheres formed, expressed as a percentage of the number of cells plated: ZsGreen-high cells versus ZsGreen-negative cells = 31% vs 9%; difference = 22%, 95% CI = 9.5% to 34.5%, $P = .01$, n = 4; Figure 1, F). The ZsGreen-high cells redistributed into ZsGreen-positive and -negative cells. By contrast, ZsGreen-negative cells formed only a few small spheres, which did not contain any ZsGreen-positive cells when analyzed by fluorescent microscopy (Figure 1, G–J).

Further immunohistochemical characterization of the ZsGreen-positive cells derived from U87MG-ZsGreen-cODC spheres revealed that they were positive for the stem cell marker nestin (Figure 2, A, and Supplementary Figure 2, E, available online), which is a substrate of the 26S proteasome (34), and negative for the differentiation markers GFAP and neuron-specific class III -tubulin (Figure 2, B and C). When U87MG-ZsGreen-cODC spheres were allowed to attach to the surface of the culture dishes and were exposed to serum-containing standard growth media (differentiating conditions), the number of ZsGreen-positive cells declined, and the attached cells became positive for GFAP and neuron-specific class III -tubulin, indicating that they had undergone differentiation (Figure 2, D–F). Similarly, spheres derived from the U343 human glioma cells stably expressing the ZsGreen-cODC reporter also expressed stem cell markers, such as Musashi-1 and Sox2 (Supplementary Figure 2, F and G, available online), in the ZsGreen-positive cells, whereas the ZsGreen-negative cells expressed the differentiation markers GFAP and TUJ-1 (Supplementary Figure 2, H and I, available online).

An important test for validating the identity of a CIC population is the demonstration of increased tumorigenicity in vivo. Therefore, the tumorigenicity of U87MG-ZsGreen-cODC cells was tested by first sorting them into ZsGreen-high and -negative populations using FACS. Different cell numbers from each population were injected subcutaneously into nude mice in numbers ranging from 10^2 to 10^6 cells per injection. Analysis of the sorted populations immediately after sorting revealed that 99.75% of ZsGreen-negative population were in fact negative for the fluorescent protein; thus, we estimated that one in 400 ZsGreen-negative cells injected was ZsGreen positive. Given that as few as 100 ZsGreen-positive cells could form a tumor (Table 1), we expected that some tumors would form in mice injected with at least 10^3 ZsGreen-negative cells and that those tumors would contain ZsGreen-positive cells. This was confirmed by in vivo fluorescent imaging, which demonstrated that some of the tumors arising from inoculation of sorted ZsGreen-negative cells contained ZsGreen-positive cells (Figure 3, C and D). Also, as mentioned above (Figure 1, G–J), ZsGreen-negative cells never repopulated into ZsGreen-positive cells in vitro (Figure 1, G–J); therefore, we concluded that

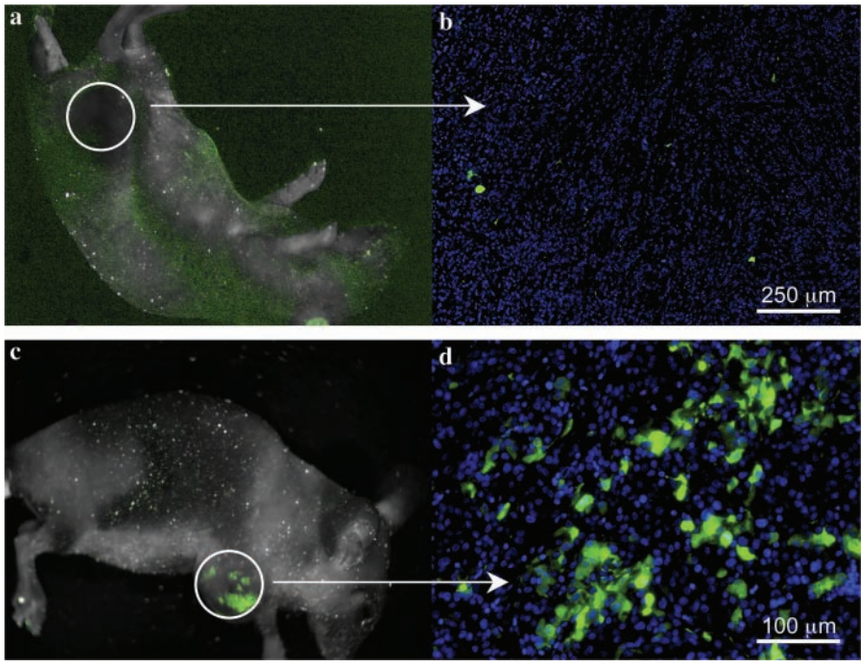

Figure 3. Tumorigenicity of cancer cells with low proteasome activity. **A, B**) ZsGreen-negative tumors derived from the ZsGreen-negative fraction of sorted sphere cells, viewed macroscopically or at high magnification. **C, D**) ZsGreen-positive tumors due to the contaminating presence of ZsGreen-positive cells in the negative fraction.

formation of a ZsGreen-positive tumor in vivo from the injection of ZsGreen-negative cells was due to the less than 100% purity of this population after sorting. Mice were inspected for tumor formation on a daily basis, and the presence of ZsGreen-positive cells was monitored by in vivo imaging for all macroscopic tumors. When we excluded tumors deriving from ZsGreen-negative cells contaminated with ZsGreen-positive cells (visible in macroscopic imaging, Figure 3, C and D) from the total number of tumors formed, we found that the ZsGreen-positive cells exhibited approximately 100-fold increased tumorigenicity compared with the ZsGreen-negative cells, suggesting that glioma cells with reduced proteasome activity are highly enriched for CICs (Table 1).

To examine if the ZsGreen-cODC reporter could be used to identify CICs in tumors, we stained sections of tumors derived from monolayer cultures of U87MG-ZsGreen-cODC cells with antibodies against the endothelial marker CD31 to identify vasculature. ZsGreen-positive cells were mainly found in perivascular regions and were absent in necrotic or avascular areas of the tumor (Supplementary Figure 3, A–C, available online). This observation was consistent with a previous report by Calabrese et al. (35), showing brain tumor stem cells to reside in a perivascular niche. In this context, it is important to note that the percentage of ZsGreen-positive cells in U87MG-ZsGreen-cODC tumors greatly exceeded the low percentage of ZsGreen-positive cells seen in vitro, which is consistent with earlier reports showing higher numbers of CICs in vivo than might be expected from in vitro observations (31).

Tracking and Targeting of CICs In Vivo Based on Proteasome Activity

These findings motivated us to test if this reporter could be used to track CICs by in vivo imaging. We recently showed that daily local fractionated irradiation (5 × 3 Gy) causes an increase in CICs numbers in vitro (13) and hypothesized that this increase was the mechanism for accelerated repopulation (36). Therefore, we mimicked this schedule in vivo. Imaging of U87MG-ZsGreen-cODC tumor-bearing mice revealed a steady increase in the fluorescent signal, which was consistent with an increase in the ZsGreen-positive cell population (Figure 4, A–D). The fact that the increase in ZsGreen fluorescence was seen 72 hours after the last fraction of radiotherapy reflects changes only in ZsGreen-positive cell numbers and not general proteasome inhibition by the radiation (18). Furthermore, the location of the positive cells near blood vessels indicated that hypoxia-induced proteasome inhibition was not a factor in the increase in ZsGreen-positive cells. These experiments demonstrate that CICs in a tumor can be imaged macroscopically in vivo and that their response to radiation therapy can be followed temporally.

The localization of ZsGreen-positive cells adjacent to blood vessels, which is traditionally thought of as a proliferative zone (37), prompted us to test if these cells were indeed proliferating, using Ki67 staining as a marker. Only a minority of ZsGreen-positive cells was also Ki67 positive (Figure 4, E). However, after sublethal fractionated irradiation (5 × 3 Gy) of tumor-bearing mice, the number of ZsGreen-positive cells in tumors increased (Figure 4, F and G) and the number of double-positive (ZsGreen-positive and Ki67-positive) cells tripled (n = 2) (Figure 4, H), suggesting that accelerated tumor repopulation may derive from the ZsGreen-positive cell compartment.

To explore if constitutive reduction of proteasome activity in CICs could be exploited therapeutically, we expressed a fusion protein consisting of TK, ZsGreen, and the cODC degron in U87MG cells. These cells were tested for sphere-forming capacity

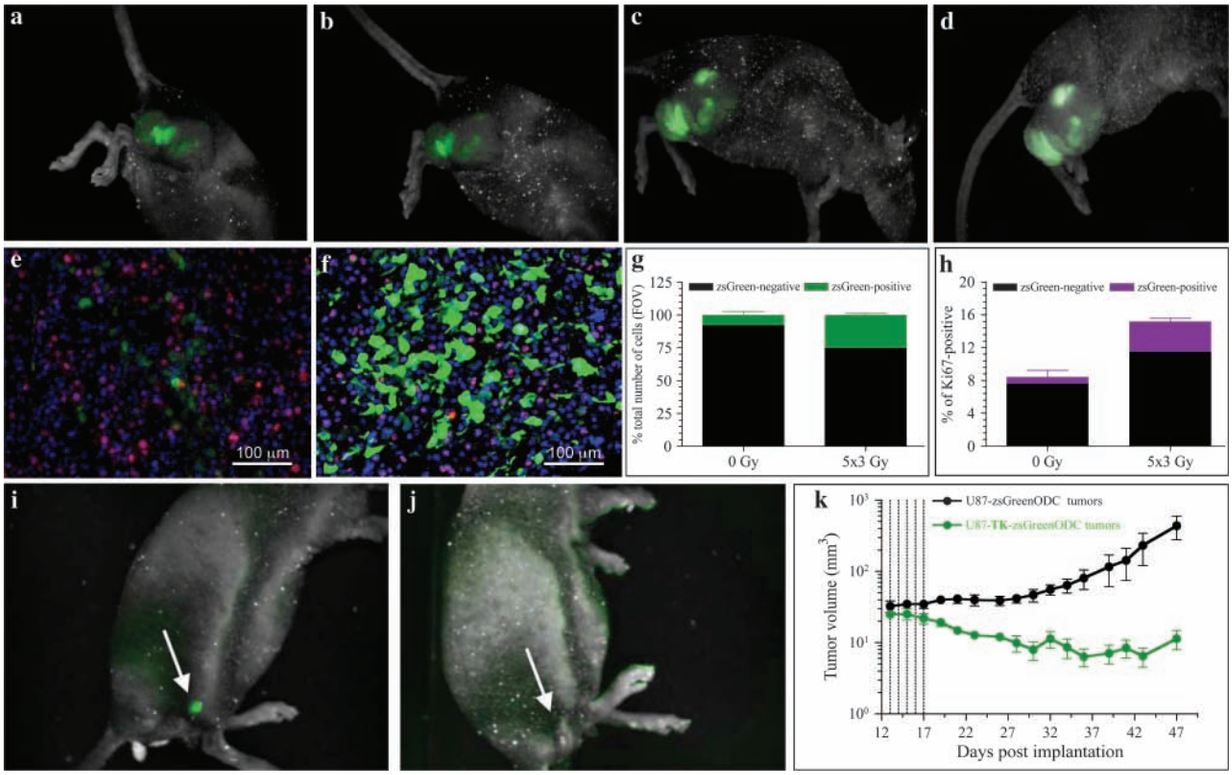

Figure 4. The effect of fractionated radiation on cancer-initiating cells in vivo. **A–D**) U87MG-ZsGreen-cODC–expressing tumors subjected to fractionated radiation and imaged before treatment (A), after a 3-Gy radiation exposure (B), after 5- × 3-Gy radiation exposures (C), or 72 hours after the last fraction (D). **E, F**) High-magnification views of untreated tumors (E), in which the proliferating, Ki67-positive population of cells displays high proteasome activity with only a few low proteasome activity (ZsGreen-positive) cells, and tumors treated with daily fractions of 3 Gy (F), in which the number of ZsGreen-positive cells increased substantially (**G**) as did the percentage of cells that were positive for Ki67 (**H**). Counterstaining with DAPI (**blue**). Mean values and 95% confidence intervals (CIs) are shown for two independent experiments. **I–K**) Mice with tumors derived from U87MG cells expressing a fusion protein of thymidine kinase, ZsGreen and the carboxyl terminus of the murine ornithine decarboxylase degron, treated with ganciclovir (5 intraperitoneal injections of 50 mg/kg starting on day 12 after implantation [**I**] and 18 days after initiation of treatment [**J**]). **K**) Growth of the tumors in the mice treated with ganciclovir. Tumor volume (mm^3) was assessed with calipers and are shown as means and 95% CIs (n = 5 mice per group).

(self-renewal) in vitro and tumor formation in vivo in the presence or absence of the TK substrate ganciclovir, which would be expected to eliminate ZsGreen-positive cells accumulating the ZsGreen-TK-cODC fusion protein. Treatment with ganciclovir selectively killed ZsGreen-positive cells, thus abrogating the sphere-forming capacity in vitro (Supplementary Figure 4, A–E, available online), and caused tumor regression in vivo (mean tumor volumes on day 48 post tumor implantation: ZsGreen-ODC tumors = 612.2 mm^3, n = 5, TK-ZsGreen-ODC tumors = 9.495 mm^3, n = 6; difference = 602.7 mm^3, 95% CI = 164.3 to 1041 mm^3, $P = .0125$, Student t test) (Figure 4, I–K).

Discussion

Here, we provide evidence that constitutively reduced 26S proteasome activity is a general feature of CICs in glioma and breast cancer cells. Consistent with this finding, Rpn2, which is thought to feed substrates into the 20S core particle (38), was nearly absent in CICs. Like normal stem cells, CICs are usually considered quiescent (39,40) with low protein turnover and reduced metabolism and thus they may not need an ATP-dependent protein degradation machinery (41).

Using a reporter construct for 26S proteasome activity, we were able to identify CICs in cell populations in vitro and in vivo. In vivo, these cells localized around blood vessels (Supplementary Figure 3, available online) consistent with a recent report by Calabrese et al. (35) showing that brain tumor stem cells reside in a perivascular niche.

Reduced proteasome activity coincided with the expression of stem cell markers and a lack of differentiation markers (Supplementary Figure 2, available online). Cells with low proteasome activity also showed increased self-renewal capacity and could form tumors in immunologically incompetent mice from as few as 100 cells (Figure 1 and Table 1). Taken together, our results indicate that the population of cells identified by reduced proteasome activity was identical or overlapped with CICs and that reduced 26S proteasome activity is a property of CICs that can cross species barriers.

Our study has several limitations. First, the fusion protein–negative cell populations in our study were not 100% pure, and purging of the remaining contaminating ZsGreen-positive cells via specific targeting with ganciclovir would have caused considerable toxicity. However, given this impurity, our study likely underestimates the difference in tumorgenicity between ZsGreen-positive

and ZsGreen-negative cells. Second, we cannot rule out the possibility that ZsGreen-negative cells can eventually become ZsGreen-positive cells. Long-term experiments that follow single cells will be necessary to address this question. Finally, like all other investigators to our knowledge, we have required approximately 100 ZsGreen-positive cells to form tumors in vivo. Therefore, it is possible that ZsGreen-positive cells need to be further purified to obtain a pure CSC population.

Although the cell population with reduced proteasome activity was noncycling in vivo, it responded to fractionated doses of ionizing radiation by rapidly undergoing proliferation. This observation suggests that regulation of proteasome function in CICs can be turned on temporarily to allow progression through the cell cycle (a gain of proteasome function would not necessarily be detected by ZsGreen-cODC which has a half-life of >3.5 hours in cells). This switch in function may be highly dependent on developmental pathways as suggested by the fact that Notch signaling–dependent increases in stem cell numbers occur after sublethal doses of fractionated radiation in breast cancer (13) and may be an indicator of accelerated repopulation observed clinically in radiation therapy (an increased tumor growth rate during gaps in radiation treatment has been described in the context of clinical radiation therapy) (36). Because accelerated repopulation of tumors is a major cause of treatment failure, tracking of CICs in vivo may facilitate the search for novel therapeutic approaches that improve radiation therapy outcome. One possible application of being able to track CICs is the use of fusion of fluorescent proteins, suicide genes, and the cODC degron in gene therapy. Similar to our experiments with cells expressing the TK-ZsGreen-ODC fusion protein, the suicide gene can be substituted for the gene of interest, whereas the fluorescent component of the reporter will allow for the tracking of the cells accumulating the suicide protein, as well as their subsequent elimination. Using a TK-ZsGreen-cODC vector, we demonstrated that CICs could be targeted specifically which led to tumor control (Figure 4).

Our observations also offer a simple explanation for the high expression levels of known stem cell markers like BMI-1 and nestin in CICs that are both substrates of the proteasome (34,42). Furthermore, because the proteasome is also responsible for the generation of peptides presented to the immune system on MHC -I molecules, our data suggest that CSCs may be immunologically silent or express antigens that may not be targeted by many current immunotherapy approaches. Finally, this system allows for screening of novel compounds that might modulate 26S proteasome function specifically in CICs, which could lead to novel targeted therapies against this therapeutically important cancer cell subpopulation.

References

1. Reya T, Morrison SJ, Clarke MF, Weissman IL. Stem cells, cancer, and cancer stem cells. *Nature.* 2001;414(6859):105–111.
2. Lagasse E. Cancer stem cells with genetic instability: the best vehicle with the best engine for cancer. *Gene Ther.* 2008;15(2):136–142.
3. Park CY, Tseng D, Weissman IL. Cancer stem cell-directed therapies: recent data from the laboratory and clinic. *Mol Ther.* 2008 .
4. Al-Hajj M, Wicha MS, Benito-Hernandez A, Morrison SJ, Clarke MF. Prospective identification of tumorigenic breast cancer cells. *Proc Natl Acad Sci USA.* 2003;100(7):3983–3988.
5. Singh SK, Hawkins C, Clarke ID, et al. Identification of human brain tumour initiating cells. *Nature.* 2004;432(7015):396–401.
6. Fang D, Nguyen TK, Leishear K, et al. A tumorigenic subpopulation with stem cell properties in melanomas. *Cancer Res.* 2005;65(20): 9328–9337.
7. Collins AT, Berry PA, Hyde C, Stower MJ, Maitland NJ. Prospective identification of tumorigenic prostate cancer stem cells. *Cancer Res.* 2005; 65(23):10946–10951.
8. Ricci-Vitiani L, Lombardi DG, Pilozzi E, et al. Identification and expansion of human colon-cancer-initiating cells. *Nature.* 2007;445(7123):111–115.
9. Prince ME, Sivanandan R, Kaczorowski A, et al. Identification of a subpopulation of cells with cancer stem cell properties in head and neck squamous cell carcinoma. *Proc Natl Acad Sci USA.* 2007;104(3):973–978.
10. Li C, Heidt DG, Dalerba P, et al. Identification of pancreatic cancer stem cells. *Cancer Res.* 2007;67(3):1030–1037.
11. Eramo A, Ricci-Vitiani L, Zeuner A, et al. Chemotherapy resistance of glioblastoma stem cells. *Cell Death Differ.* 2006;13(7):1238–1241.
12. Bao S, Wu Q, McLendon RE, et al. Glioma stem cells promote radioresistance by preferential activation of the DNA damage response. *Nature.* 2006;444(7120):756–760.
13. Phillips TM, McBride WH, Pajonk F. The response of CD24(/low)/ CD44+ breast cancer-initiating cells to radiation. *J Natl Cancer Inst.* 2006; 98(24):1777–1785.
14. Pajonk F, McBride WH. The proteasome in cancer biology and treatment. *Radiat Res.* 2001;156(5):447–459.
15. Cusack JC Jr, Liu R, Houston M, et al. Enhanced chemosensitivity to CPT-11 with proteasome inhibitor PS-341: implications for systemic nuclear factor-kappaB inhibition. *Cancer Res.* 2001;61(9):3535–3540.
16. Pajonk F, Pajonk K, McBride WH. Apoptosis and radiosensitization of Hodgkin cells by proteasome inhibition. *Int J Radiat Oncol Biol Phys.* 2000;47(4):1025–1032.
17. Pajonk F, van Ophoven A, Weissenberger C, McBride WH. The proteasome inhibitor MG-132 sensitizes PC-3 prostate cancer cells to ionizing radiation by a DNA-PK-independent mechanism. *BMC Cancer.* 2005;5(1): 76.
18. Pajonk F, McBride WH. Ionizing radiation affects 26s proteasome function and associated molecular responses, even at low doses. *Radiother Oncol.* 2001;59(2):203–212.
19. Fekete MR, McBride WH, Pajonk F. Anthracyclines, proteasome activity and multi-drug-resistance. *BMC Cancer.* 2005;5(1):114.
20. Piccinini M, Tazartes O, Mezzatesta C, et al. Proteasomes are a target of the anti-tumor drug vinblastine. *Biochem J.* 2001;356(pt 3):835–841 .
21. Pajonk F, van Ophoven A, McBride WH. Hyperthermia-induced proteasome inhibition and loss of androgen receptor expression in human prostate cancer cells. *Cancer Res.* 2005;65(11):4836–4843.
22. Kane RC, Bross PF, Farrell AT, Pazdur R. Velcade: U.S. FDA approval for the treatment of multiple myeloma progressing on prior therapy. *Oncologist.* 2003;8(6):508–513.
23. Blaney SM, Bernstein M, Neville K, et al. Phase I study of the proteasome inhibitor bortezomib in pediatric patients with refractory solid tumors: a Children's Oncology Group study (ADVL0015). *J Clin Oncol.* 2004;22(23): 4752–4757.
24. Davis NB, Taber DA, Ansari RH, et al. Phase II trial of PS-341 in patients with renal cell cancer: a University of Chicago phase II consortium study. *J Clin Oncol.* 2004;22(1):115–119.
25. Gomez-Abuin G, Winquist E, Stadler WM, et al. A phase II study of PS-341 (Bortezomib) in advanced or metastatic urothelial cancer. A trial of the Princess Margaret Hospital and University of Chicago phase II consortia. *Invest New Drugs.* 2007;25(2):181–185.
26. Kondagunta GV, Drucker B, Schwartz L, et al. Phase II trial of bortezomib for patients with advanced renal cell carcinoma. *J Clin Oncol.* 2004; 22(18):3720–3725.
27. Shah MH, Young D, Kindler HL, et al. Phase II study of the proteasome inhibitor bortezomib (PS-341) in patients with metastatic neuroendocrine tumors. *Clin Cancer Res.* 2004;10(18 pt 1):6111–6118.
28. Reynolds BA, Tetzlaff W, Weiss S. A multipotent EGF-responsive striatal embryonic progenitor cell produces neurons and astrocytes. *J Neurosci.* 1992;12(11):4565–4574.

29. Glas R, Bogyo M, McMaster JS, Gaczynska M, Ploegh HL. A proteolytic system that compensates for loss of proteasome function. *Nature.* 1998; 392(6676):618–622.
30. Matsuzawa S, Cuddy M, Fukushima T, Reed JC. Method for targeting protein destruction by using a ubiquitin-independent, proteasome-mediated degradation pathway. *Proc Natl Acad Sci USA.* 2005;102(42): 14982–14987.
31. Hemmati HD, Nakano I, Lazareff JA, et al. Cancerous stem cells can arise from pediatric brain tumors. *Proc Natl Acad Sci USA.* 2003;100(25): 15178–15183.
32. Ponti D, Costa A, Zaffaroni N, et al. Isolation and in vitro propagation of tumorigenic breast cancer cells with stem/progenitor cell properties. *Cancer Res.* 2005;65(13):5506–5511.
33. Hernebring M, Brolen G, Aguilaniu H, Semb H, Nystrom T. Elimination of damaged proteins during differentiation of embryonic stem cells. *Proc Natl Acad Sci USA.* 2006;103(20):7700–7705.
34. Mellodew K, Suhr R, Uwanogho DA, et al. Nestin expression is lost in a neural stem cell line through a mechanism involving the proteasome and Notch signalling. *Brain Res Dev Brain Res.* 2004;151(1–2):13–23.
35. Calabrese C, Poppleton H, Kocak M, et al. A perivascular niche for brain tumor stem cells. *Cancer Cell.* 2007;11(1):69–82.
36. Withers HR, Maciejewski B, Taylor JM, Hliniak A. Accelerated repopulation in head and neck cancer. *Front Radiat Ther Oncol.* 1988;22:105–110 . **Q31**
37. Tannock IF. Population kinetics of carcinoma cells, capillary endothelial cells, and fibroblasts in a transplanted mouse mammary tumor. *Cancer Res.* 1970;30(10):2470–2476.
38. Rosenzweig R, Osmulski PA, Gaczynska M, Glickman MH. The central unit within the 19S regulatory particle of the proteasome. *Nat Struct Mol Biol.* 2008 . **Q32**
39. Holtz MS, Forman SJ, Bhatia R. Nonproliferating CML CD34+ progenitors are resistant to apoptosis induced by a wide range of proapoptotic stimuli. *Leukemia.* 2005;19(6):1034–1041.
40. Holtz M, Forman SJ, Bhatia R. Growth factor stimulation reduces residual quiescent chronic myelogenous leukemia progenitors remaining after imatinib treatment. *Cancer Res.* 2007;67(3):1113–1120.
41. Babbitt SE, Kiss A, Deffenbaugh AE, et al. ATP hydrolysis-dependent disassembly of the 26S proteasome is part of the catalytic cycle. *Cell.* 2005;121(4):553–565.
42. Ben-Saadon R, Zaaroor D, Ziv T, Ciechanover A. The polycomb protein Ring1B generates self atypical mixed ubiquitin chains required for its in vitro histone H2A ligase activity. *Mol Cell.* 2006;24(5):701–711.

Funding

E. Vlashi was supported by a training grant from the National Institute of Biomedical Imaging and BioEngineering (2 T32 EB002101-31). This work was supported by a grant from the Department of Defense (PC060599), by a grant of the California Breast Cancer Research Program (BC060077), and by a developmental grant from the In Vivo Cellular and Molecular Imaging Centre at University of California, Los Angeles (PI: H. Herschman, NIH P50CA08630608) to F. Pajonk.

Notes

The authors are grateful for the excellent technical support provided by the staff of the Defined Flora animal facility of the Department of Radiation Oncology at the University of California, Los Angeles. The authors take full responsibility for the study design; collection, analysis, and interpretation of the data; the decision to submit the manuscript for publication; and the writing of the manuscript.

Manuscript received July 3, 2008; revised November 24, 2008; accepted December 31, 2008.